ELSEVIER

International Journal of Solids and Structures 41 (2004) 1357–1375

INTERNATIONAL JOURNAL OF SOLIDS and STRUCTURES

www.elsevier.com/locate/ijsolstr

# A finite element based on cubic zig-zag plate theory for the prediction of thermo-electric-mechanical behaviors

Jinho Oh, Maenghyo Cho *

*School of Mechanical and Aerospace Engineering, Seoul National University, San 56-1, Shillim-Dong, Kwanak-Gu, Seoul 151-744, South Korea*

Received 8 June 2003; received in revised form 20 October 2003

**Abstract**

A three-node triangular finite element based on cubic zig-zag plate theory is developed to refine the predictions of the mechanical, thermal, and electric behaviors fully coupled. Both the displacement and temperature fields through the thickness are constructed by superimposing linear zig-zag field to the smooth globally cubic varying field. Smooth parabolic distribution through the thickness is assumed in the transverse deflection in order to consider transverse normal deformation. Linear zig-zag form is adopted in the electric field. The layer-dependent degrees of freedom of displacement and temperature fields are expressed in terms of reference primary degrees of freedom by applying interface continuity conditions as well as bounding surface conditions of transverse shear stresses and transverse heat flux. This non-conforming element passes the bending patch tests in arbitrary mesh configurations. Non-conforming C1 shape functions for the variables of out-of-plane displacement field are introduced. Nodal variables are displacements, temperature, and elastic potentials. Through the numerical examples of coupled and uncoupled analysis, the accuracy and efficiency of the present finite element are demonstrated. For the improvement of accuracy of interlaminar stresses, post-processing approach of integration of equilibrium equation is used. For the computation of higher order derivatives in the 3-D stress equilibrium equations, differential quadrature method is employed. The present finite element is suitable in the predictions of fully coupled behaviors of thick smart composite plate under mechanical, thermal, and electric loadings.


*Keywords:* Finite element; Zig-zag plate theory; Transverse stresses; Non-conforming C1 shape function; Differential quadrature; Coupled behavior; Thermo-electric-mechanical behavior

## 1. Introduction

In recent years, development of integration of piezo-electric materials to composite structures is paid special attentions due to their smart structural functionality as sensors and actuators. Thus it is important to model and predict the behaviors of smart composite structures in the critical situations. Especially the

* Corresponding author. Fax: +82-2-886-1693.
*E-mail address:* mhcho@snu.ac.kr (M. Cho).

0020-7683/$ - see front matter © 2003 Elsevier Ltd. All rights reserved.
doi:10.1016/j.ijsolstr.2003.10.019

full coupling effects need to be investigated in the study of smart structures in high temperature environment. Among the possible approaches, 3-dimensional and quasi-3-dimensional models are not computationally tractable. Thus many researchers are pursuing more efficient methods to accurately analyze many-layered smart structures.

In the early stage of the development of models, classical/first order shear deformation theory has been employed to predict mechanical behavior of embedded or surface bonded piezo-electric layers (Crawley, 1987; Lee, 1990). The finite elements based on the smart classical/first order plate theories have been developed for the application to general shape and loading conditions (Ha et al., 1992).

However, for the accurate prediction of static and dynamic behavior for general layup configurations of smart laminated structures, classical and first order shear theories are not adequate. Thus higher order theories with smeared displacements and layerwise electric potential fields (Mitchell and Reddy, 1995; Franco Correia et al., 2000) and full layerwise theories and corresponding finite element have been developed by Saravanos et al. (1997). The smeared theory is not sufficient to describe the deformation behavior through the thickness because it cannot satisfy static continuity conditions at the interfaces between layers. Layerwise theory can adequately describe the deformation behavior through the thickness but it is not computationally efficient because it employs a large number of degrees of freedom which depend upon the number of layers (Reddy and Robbins, 1994).

In thermo-mechanical problem, even in moderate thick plate configurations, the transverse normal deformation effect cannot be neglected since the effect of out-of-plane thermal deformation is equally important compared to those of the in-plane thermal deformations (Ali et al., 1999). In addition, for the reliable analysis of adaptive composite laminates under thermal environments, full coupling effects between thermal-mechanical-electricity should be considered. Chattopadhyay et al. (1999) used a finite element model based on the smeared cubic higher order theory to analyze the smart structures with the full coupling of thermo-mechanical-electricity. However, smeared theories are not adequate in the prediction of deformation behavior and layerwise models and 3-D solid models are computationally too expensive. Thus it is still required to develop accurate and efficient model and corresponding finite element that can predict the static and dynamic behaviors of smart structures under thermo-electric-mechanical coupled situations.

In the present study, we aim at developing a plate bending element which is based on higher order zig-zag theory (Cho and Oh, 2001, submitted for publication) for the prediction of fully coupled behavior of smart composite plates under the thermo-electric-mechanical environments. To predict reliable deformation behaviors, transverse normal as well as transverse shear deformations are considered. For the efficient evaluation of the mechanical behaviors, transverse shear stress balance conditions are pre-imposed in the displacement field to reduce total active degrees of freedom. The temperature field is also obtained by superimposing linear zig-zag field into the global smeared cubic field. The layer-dependent temperature degrees of freedom are suppressed by imposing top and bottom surface heat flux conditions as well as interface transverse heat flux continuity conditions. The formulation includes full coupling between thermo-mechanical-electric behaviors. Even though the developed theory is a two-dimensional plate version, full three-dimensional constitutive equations are used for the accurate prediction of the deformation under thermal and electric loads combined.

The developed finite element does not have layer-dependent degrees of freedom of displacement field and temperature field but it has layer-dependent degrees of freedom for electric potentials in order to describe arbitrary distributions of electric potential through the thickness of smart structures.

## 2. Zig-zag model review

The free energy density function may be written as follows and can be found in Chattopadhyay et al. (1999):

$$F(\varepsilon_{ij}, E_i, \theta) = \frac{1}{2} C_{ijkl}\varepsilon_{ij}\varepsilon_{kl} - e_{ijk}E_i\varepsilon_{jk} - \frac{1}{2} b_{ij}E_iE_j - k_{ij}\theta\varepsilon_{ij} - d_iE_i\theta - \frac{1}{2} a_T\theta^2 \tag{1}$$

where the quantities $C_{ijkl}$, $e_{ijk}$, and $C_E$ are the elastic constants, the piezoelectric constants, and the heat capacity respectively, and $a_T$ is defined as $C_E/T_0$.

The constitutive equations for fully coupled thermo-mechanical-electric materials are given as

$$\sigma_{ij} = \frac{\partial F}{\partial \varepsilon_{ij}} = C_{ijkl}\varepsilon_{kl} - e_{ijk}E_k - k_{ij}\theta \tag{2}$$

$$D_i = -\frac{\partial F}{\partial E_i} = e_{ijk}\varepsilon_{jk} + b_{ij}E_j + d_i\theta \tag{3}$$

$$S = -\frac{\partial F}{\partial \theta} = k_{ij}\varepsilon_{ij} + d_iE_i + a_T\theta \tag{4}$$

where $\sigma_{ij}$ and $D_i$ are the components of the stress tensor and electric displacement vector. $S$ denotes entropy. $\theta = T - T_0$ is the temperature rise from the initial temperature $T_0$. $E_i$ is the components of the electric field vector. $b_{ij}$ is the dielectric permittivity and $k_{ij}$ and $d_i$ refer to the thermal-mechanical and the thermal-piezoelectric coupling constants.

In the case of considering partial coupling, the constitutive equation given in Eq. (2) is used only for the analysis. Based on linear piezoelectricity, $E_i$ can be expressed from a scalar potential function $\phi$ as follows:

$$E_i = -\phi_{,i} \quad (i = 1, 2, 3) \tag{5}$$

Infinitesimal displacement and strain relationship is used and it is given as

$$\varepsilon_{ij} = \frac{1}{2}(u_{i,j} + u_{j,i}) \tag{6}$$

The configuration of the smart laminated composite plate is shown in Fig. 1.

For efficient modeling without losing the accuracy in the present study, a fully coupled higher-order zig-zag theory is proposed. A zig-zag higher order in-plane displacement field is obtained by superimposing zig-zag linear field to the globally cubic varying field. In order to include the transverse normal effect which is significant in thermo-mechanical problems, the out-of-plane displacement field is assumed as globally parabolic form through the thickness.

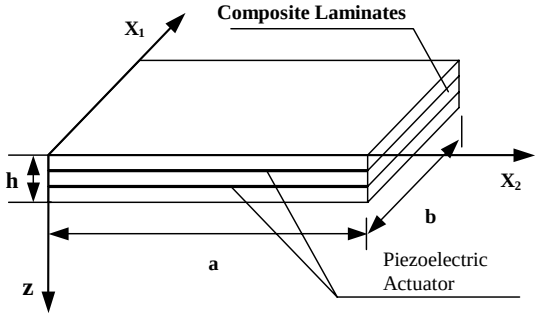


Fig. 1. Configuration of the adaptive laminated composite plates.

The starting displacement field can be written as follows:

$$\begin{aligned} u_\alpha(x_\beta, z) &= u_\alpha^o(x_\beta) + \psi_\alpha(x_\beta)z + \xi_\alpha(x_\beta)z^2 + \varphi_\alpha(x_\beta)z^3 + \sum_{k=1}^{N-1} S_\alpha^k(x_\beta)(z - z_k)H(z - z_k) \\ u_3(x_\alpha, z) &= w(x_\alpha) + r_1(x_\alpha)z + r_2(x_\alpha)z^2 \end{aligned} \tag{7}$$

where $H(z - z_k)$ is a Heaviside unit step function.

By applying top and bottom surface transverse shear free conditions, and applying transverse shear stress continuity conditions at the interface between layers, the final displacement field reduces to the following form.

$$\begin{aligned} u_\alpha(x_\beta, z, t) &= u_\alpha^o(x_\beta, t) - w_{,\alpha}(x_\beta, t)z - \frac{1}{2h}\left\{ 3\varphi_\alpha h^2 + \sum_{k=1}^{N-1}\left(a_{\alpha\gamma}^k \varphi_\gamma + b_{\alpha\gamma}^k r_{2,\gamma}\right) + r_{1,\alpha}(x_\beta, t)h + r_{2,\alpha}(x_\beta, t)h^2 \right\} z^2 \\ &\quad + \varphi_\alpha(x_\beta, t)z^3 + \sum_{k=1}^{N-1}\left(a_{\alpha\gamma}^k \varphi_\gamma + b_{\alpha\gamma}^k r_{2,\gamma}\right)(z - z_k)H(z - z_k) \\ u_3(x_\alpha, z, t) &= w(x_\alpha, t) + r_1(x_\alpha, t)z + r_2(x_\alpha, t)z^2 \end{aligned} \tag{8}$$

The detailed derivation can be found in Cho and Oh (2001, 2002).

The variables in the final displacement field are defined only at the reference plane. The primary variables are $u_\alpha^0$, $w$, $\varphi_\alpha$, $r_1$, $r_2$. Thus the number of the primary variables does not depend upon the number of layers.

Similar to the displacement field construction, the temperature field through the thickness of the plate is obtained by superimposing linear zig-zag field onto the global cubic smooth field. The starting temperature field can be written as follows:

$$\theta(x_\beta, z, t) = \theta_0(x_\beta, t) + \theta_1(x_\beta, t)z + \theta_2(x_\beta, t)z^2 + \theta_3(x_\beta, t)z^3 + \sum_{k=1}^{N-1} \theta^{sk}(x_\beta, t)(z - z_k)H(z - z_k) \tag{9}$$

In general, the plate may be subjected to either thermal loads or prescribed temperature at both top and bottom surfaces. Four different set of bounding surface conditions may be considered and they were given in Cho and Oh (submitted for publication). In the present study, we focus on the case of thermal heat flux applied on the bounding surfaces. Thus the two thermal boundary conditions on both surfaces are expressed as

$$\begin{cases} -\kappa_{33}^1 \theta_{,Z} = q_\mathrm{t} & \text{at } z = 0 \\ -\kappa_{33}^N \theta_{,Z} = q_\mathrm{b} & \text{at } z = h \end{cases} \tag{10}$$

By applying the heat flux conditions on top and bottom surfaces and applying transverse heat flux continuity condition at each interface between layers, the expression for the temperature field can be written as follows:

$$\begin{aligned} \theta &= \theta_0 - \frac{q_\mathrm{t}}{\kappa_{33}^1} z - \frac{1}{2h}\left\{ \frac{q_\mathrm{b}}{\kappa_{33}^N} - \frac{q_\mathrm{t}}{\kappa_{33}^1} + 3\theta_3 h^2 + \sum_{k=1}^{N-1}(C^k\theta_3 + d^k) \right\} z^2 + \theta_3 z^3 \\ &\quad + \sum_{k=1}^{N-1}(C^k\theta_3 + d^k)(z - z_k)H(z - z_k) \end{aligned} \tag{11}$$

where $q_\mathrm{t}$ and $q_\mathrm{b}$ indicate the heat flux applied on top and bottom surfaces, respectively. $\kappa_{33}^i$ denotes the thermal conductivity in the thickness direction in the $i$th layer. It must be noted that the higher order

temperature field defines a non-uniform zig-zag temperature distribution through the thickness of plates. The functions $\theta_0(x_\beta)$ and $\theta_3(x_\beta)$ define the in-plane temperature variations. The detailed expressions for the coefficients of Eq. (11) can be found in Cho and Oh (2001, submitted for publication). It is important to note that although a linear temperature field can address the in-plane temperature distribution, it cannot satisfy the surface thermal boundary conditions nor the heat flux continuity conditions at the interfaces between layers. Therefore, temperature variations through the thickness, which produce the most important bending deformation, cannot be modeled accurately by the linear temperature field nor smooth cubic field. The present temperature field given in Eq. (11) can describe accurate and simple distribution through the thickness and the pattern is consistent with the displacement field given in Eq. (8). It should be emphasized that if the adjacent layers have severe changes of thermal material properties like sandwich plates or hybrid composite plates, the temperature field given in Eq. (11) can predict accurate but significantly different results from those of smeared temperature fields.

The expressions for the potential function can be written as follows:

$$\phi = \sum_{k=1}^{N} \left\{ \phi_0^{(k)} + \phi_1^{(k)}(z - z_{k-1}) \right\} \{ H(z - z_{k-1}) - H(z - z_k) \} \tag{12}$$

The descriptions of the electric potential $\phi$ are expressed as layer-dependent form using linear zig-zag field through the thickness. Two degrees of freedom are required to express electric potential $\phi$ in each layer. Even though the layer-dependent potential field is assumed through the thickness, the number of piezo-layers is relatively small compared to the total number of layers. Thus this layer-dependent electric potential field does not increase the number of degrees of freedom significantly. Variational functional based on Eqs. (8), (11) and (12) can be constructed for general materials with fully coupled constitutive relations given in Eqs. (2)–(4). The equilibrium equations and boundary conditions can be derived from the Hamilton principle. The fully coupled governing equations for the proposed deformation, temperature, and electric field can be derived in a straightforward way and it was derived in Cho and Oh (submitted for publication).

## 3. Formulation of a non-conforming finite element method

The laminated plate theory which we have developed has second derivatives of $w$ (transverse deflection at the reference plane) and $r_1$ and $r_2$ in the expression of strain energy. Thus $C^1$ (slope-continuous) functions should be used. However, it is well known in plate theory that it is difficult to impose $C^1$ conditions at the interfaces between elements (in $x$–$y$ plane) in an arbitrary mesh configuration. In the present study, a triangular plate bending element is developed for its simplicity and expediency in modeling arbitrary boundary shapes. The thin plate non-conforming triangular element developed by Specht (1988) satisfies $C^1$ condition at the nodes, but not along element boundaries. This element is the starting point for our development.

In the finite element formulation, the coordinates $x$ and $y$ indicates $x_1$ and $x_2$, respectively. For the present three-noded triangular element, the nodal displacement vector $\{a\}^e$ is $\{u_{xi}^o, u_{yi}^o, \varphi_{xi}, \varphi_{yi}, w_i, \theta_{xi}, \theta_{yi}, r_{1i}, R_{1xi}, R_{1yi}, r_{2i}, R_{2xi}, R_{2yi}, \phi_0, \phi_1, \theta_0, \theta_3\}$ where $\theta_x = w_{,y}$ and $\theta_y = -w_{,x}$ and $R_{1x} = r_{1,y}$ and $R_{1y} = -r_{1,x}$ and $R_{2x} = r_{2,y}$ and $R_{2y} = -r_{2,x}$. Area coordinates $L_1$, $L_2$, and $L_3$ are used as interpolation functions. The detailed geometry and the coordinates for the triangular element is shown in Fig. 2.

The global coordinates are expressed as follows:

$$x = \sum_{i=1}^{3} L_i x_i, \quad y = \sum_{i=1}^{3} L_i y_i \tag{13}$$

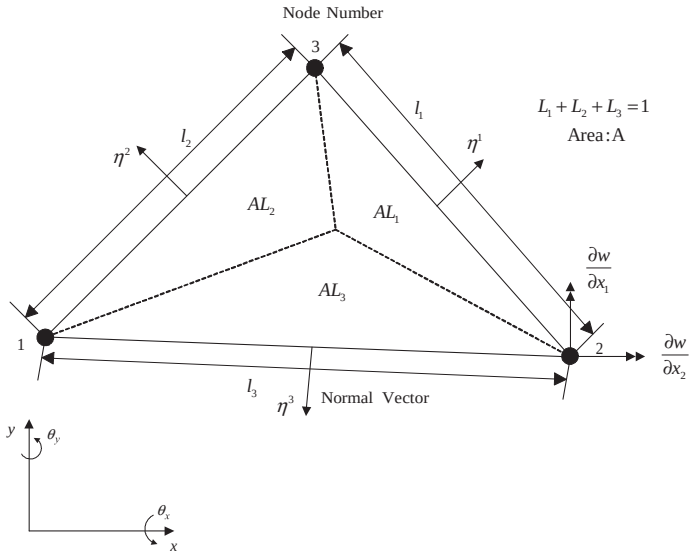


Fig. 2. Geometry and coordinates for the triangular element.

Isoparametric mapping is used for displacement unknowns $u_x^o$, $u_y^o$, $\varphi_x^o$, $\varphi_y^o$, $\phi_0$, $\phi_1$, $\theta_0$, and $\theta_3$. Subparametric mapping is used for $w$, $r_1$, and $r_2$. The primary displacement unknowns are expressed in terms of nodal variables and shape functions as follows:

$$u_x^o = \sum_{i=1}^{3} L_i u_{xi}^o, \quad u_y^o = \sum_{i=1}^{3} L_i u_{yi}^o \tag{14}$$

$$\varphi_x^o = \sum_{i=1}^{3} L_i \varphi_{xi}^o, \quad \varphi_y^o = \sum_{i=1}^{3} L_i \varphi_{yi}^o \tag{15}$$

$$w = \sum_{i=1}^{3} \{w_i N_i + \theta_{xi} N_{xi} + \theta_{yi} N_{yi}\} \tag{16}$$

$$r_1 = \sum_{i=1}^{3} \{r_{1i} N_i + R_{1xi} N_{xi} + R_{1yi} N_{yi}\}, \quad r_2 = \sum_{i=1}^{3} \{r_{2i} N_i + R_{2xi} N_{xi} + R_{2yi} N_{yi}\} \tag{17}$$

$$\phi_0 = \sum_{i=1}^{3} L_i \phi_{0i}, \quad \phi_1 = \sum_{i=1}^{3} L_i \phi_{1i} \tag{18}$$

$$\theta_0 = \sum_{i=1}^{3} L_i \theta_{0i}, \quad \theta_3 = \sum_{i=1}^{3} L_i \theta_{3i} \tag{19}$$

where the detailed expressions for $N_i$, $N_{xi}$, $N_{yi}$ are taken from Specht (1988). The terms of the basis of shape functions in the area coordinate system are reproduced here, with corrections of errors made in Specht (1988). It can also be found in Cho and Parmerter (1994).

$$N_i = n_{3i-2}, \quad N_{xi} = n_{3i-1}, \quad N_i = n_{3i} \tag{20}$$

where $i = 1$, 2, and 3.

The shape functions can be written in the form

$$n_a = \sum_{r=1}^{9} Z_{ar}^{-1} z_r \tag{21}$$

where $a = 1, \ldots, 9$

$$\begin{aligned}[z_r] = \Bigg[ & L_1, L_2, L_3, L_1L_2, L_2L_3, L_3L_1, L_1^2L_2 + \frac{1}{2}L_1L_2L_3\{3(1-\mu_3)L_1 - (1+3\mu_3)L_2 + (1+3\mu_3)L_3\}, \\ & L_2^2L_3 + \frac{1}{2}L_1L_2L_3\{3(1-\mu_1)L_2 - (1+3\mu_1)L_3 + (1+3\mu_1)L_1\}, \\ & L_3^2L_1 + \frac{1}{2}L_1L_2L_3\{3(1-\mu_2)L_3 - (1+3\mu_2)L_1 + (1+3\mu_2)L_2\}\Bigg]\end{aligned} \tag{22}$$

The constants are

$$\mu_1 = \frac{l_3^2 - l_2^2}{l_1^2}, \quad \mu_2 = \frac{l_1^2 - l_3^2}{l_2^2}, \quad \mu_3 = \frac{l_2^2 - l_1^2}{l_3^2} \tag{23}$$

where $l_1$, $l_2$, and $l_3$ are the lengths of the side of the triangle.

The determination of $z_7$, $z_8$, and $z_9$ is based on the following consideration. From the boundary conditions in equation, the energy associated with interelement jumps can be written

$$\Delta U_\Gamma = \int_{\Gamma_s} M_{nn} \Delta\left(\frac{\partial w}{\partial n}\right) \mathrm{d}\Gamma + \int_{\Gamma_s} M_{ns} \Delta\left(\frac{\partial w}{\partial s}\right) \mathrm{d}\Gamma \tag{24}$$

Physically, there should be no energy associated with these interelement discontinuities; so we set both terms of Eq. (24) to zero (see Fig. 3). Since $w(s)$ is uniquely determined from the two node data, $\Delta w_{,s}$ is equal to zero.

For a constant state of bending moments, the following condition should be required to pass the bending patch test.

$$M_{nn} \int_{\Gamma_s} \Delta\left(\frac{\partial w}{\partial n}\right) \mathrm{d}\Gamma = 0 \tag{25}$$

Thus the quartic polynomials $z_7$, $z_8$, and $z_9$ are determined to satisfy Eq. (25).

The transformation matrix $Z_{ar}$ is regular for an arbitrary geometry of the triangle. The shape function $n_a$ can now be set up by Eq. (21) using the inverse transformation matrix.

$$Z_{ar}^{-1} = \begin{bmatrix} 1 & 0 & 0 & -1 & 0 & 1 & 2 & 0 & -2 \\ 0 & 0 & 0 & 0 & 0 & a_{12} & -a_{13} & 0 & -a_{12} \\ 0 & 0 & 0 & 0 & 0 & a_{22} & -a_{23} & 0 & -a_{22} \\ 0 & 1 & 0 & 1 & -1 & 0 & -2 & 2 & 0 \\ 0 & 0 & 0 & a_{13} & 0 & 0 & -a_{13} & -a_{11} & 0 \\ 0 & 0 & 0 & a_{23} & 0 & 0 & -a_{23} & -a_{21} & 0 \\ 0 & 0 & 1 & 0 & 1 & -1 & 0 & -2 & 2 \\ 0 & 0 & 0 & 0 & a_{11} & 0 & 0 & -a_{11} & -a_{12} \\ 0 & 0 & 0 & 0 & a_{21} & 0 & 0 & -a_{21} & -a_{22} \end{bmatrix}$$

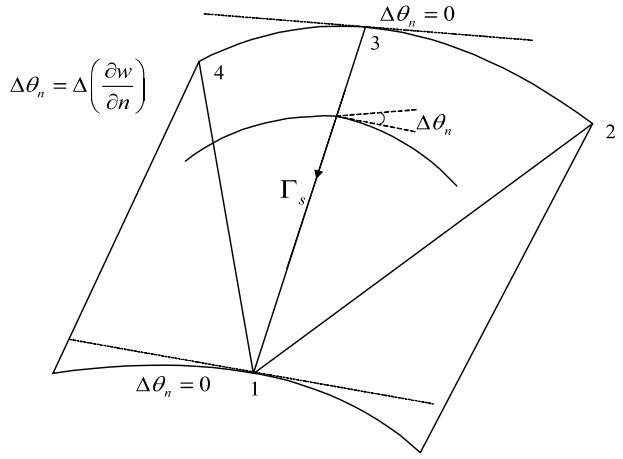


At the Node Points 1, and 3 Normal Slopes are Continuous.

Normal Slope Discontinuity Occurs at the Interface 1-3

$$\int_{\Gamma_s} M_{nn}\Delta\left(\frac{\partial w}{\partial n}\right)d\Gamma = 0$$

For Constant State of Bending Moment $M_{nn}$

$$\int_{\Gamma_s} \Delta\left(\frac{\partial w}{\partial n}\right)d\Gamma = 0$$

Fig. 3. Element interface slope discontinuity.

where $[a_{ij}] = \left[2A\frac{\partial L_j}{\partial x_i}\right] = \begin{bmatrix} y_2 - y_3 & y_3 - y_1 & y_1 - y_2 \\ x_3 - x_2 & x_1 - x_3 & x_2 - x_1 \end{bmatrix}$ which is expressed in terms of the coordinates $(x_i, y_i)$ of the corner nodes.

In the calculation of the normal derivatives,

$$\frac{\partial}{\partial \eta^1} = \frac{l_1}{4A}\left\{\frac{\partial}{\partial L_2} + \frac{\partial}{\partial L_3} - 2\frac{\partial}{\partial L_1} + \mu_1\left(\frac{\partial}{\partial L_3} - \frac{\partial}{\partial L_2}\right)\right\} \tag{26}$$

$$\frac{\partial}{\partial \eta^2} = \frac{l_2}{4A}\left\{\frac{\partial}{\partial L_3} + \frac{\partial}{\partial L_1} - 2\frac{\partial}{\partial L_2} + \mu_2\left(\frac{\partial}{\partial L_1} - \frac{\partial}{\partial L_3}\right)\right\} \tag{27}$$

$$\frac{\partial}{\partial \eta^3} = \frac{l_3}{4A}\left\{\frac{\partial}{\partial L_1} + \frac{\partial}{\partial L_2} - 2\frac{\partial}{\partial L_3} + \mu_3\left(\frac{\partial}{\partial L_2} - \frac{\partial}{\partial L_1}\right)\right\} \tag{28}$$

where $\eta^1$, $\eta^2$, and $\eta^3$ are the normal directions of each sides of the triangle.

Strain, electric field, and temperature can be discretized and interpolated using Eqs. (5), (6) and (14)–(19). Substituting these discretized expressions into Eq. (1) and Using the Hamilton's principle, the following coupled discrete equations are obtained.

$$\begin{aligned}
&\int_0^{t_0}\int_V \rho N_u^{\mathrm{T}} N_u \,\mathrm{d}V\{\ddot{a}\}^e + \int_0^{t_0}\int_V \gamma N_u^{\mathrm{T}} N_u \,\mathrm{d}V\{\dot{a}\}^e + \int_0^{t_0}\int_V B_u^{\mathrm{T}}[QB_u + eB_\phi - kN_\theta]\,\mathrm{d}V\{a\}^e \\
&\quad = \int_0^{t_0}\int_S P_u - P_{u\theta}\,\mathrm{d}S \\
&\int_0^{t_0}\int_V B_\phi^{\mathrm{T}}[e^{\mathrm{T}}B_u - bB_\phi + dN_\theta]\,\mathrm{d}V\{a\}^e = \int_0^{t_0}\int_S P_\phi - P_{\phi\theta}\,\mathrm{d}V \\
&\int_0^{t_0}\int_V B_\theta^{\mathrm{T}}\kappa B_\theta \,\mathrm{d}V\{a\}^e + \int_0^{t_0}\int_V N_\theta^{\mathrm{T}}[kB_u + dB_\phi + aN_\theta]\,\mathrm{d}V\{\dot{a}\}^e = \int_0^{t_0}\int_S P_\theta - P_{\theta\theta}\,\mathrm{d}V
\end{aligned} \tag{29}$$

where $B_u$, $B_\phi$, and $B_\theta$ are strain–displacement, electric field-potential, and heat flux-temperature transformation matrix respectively. The components of these matrices consist of the spatial derivatives of finite element shape functions. It is omitted here for the limited space.

For the steady state response, time dependent terms are eliminated. Then the following coupled linear equations can be obtained in element level.

$$\begin{aligned}
&\int_V B_u^{\mathrm{T}}[QB_u + eB_\phi - kN_\theta]\,\mathrm{d}V\{a\}^e = \int_S P_u - P_{u\theta}\,\mathrm{d}S \\
&\int_V B_\phi^{\mathrm{T}}[e^{\mathrm{T}}B_u - bB_\phi + dN_\theta]\,\mathrm{d}V\{a\}^e = \int_S P_\phi - P_{\phi\theta}\,\mathrm{d}V \\
&\int_V B_\theta^{\mathrm{T}}\kappa B_\theta \,\mathrm{d}V\{a\}^e = \int_S P_\theta - P_{\theta\theta}\,\mathrm{d}V
\end{aligned} \tag{30}$$

The element matrices and vectors are defined by

$$\begin{aligned}
&K_{uu} = \int_V B_u^{\mathrm{T}} Q B_u \,\mathrm{d}V, \quad K_{u\phi} = \int_V B_u^{\mathrm{T}} e B_\phi \,\mathrm{d}V, \quad K_{u\theta} = \int_V B_u^{\mathrm{T}} k N_\theta \,\mathrm{d}V, \quad K_{\phi u} = \int_V B_\phi^{\mathrm{T}} e^{\mathrm{T}} B_u \,\mathrm{d}V \\
&K_{\phi\phi} = \int_V B_\phi^{\mathrm{T}} b B_\phi \,\mathrm{d}V, \quad K_{\phi\theta} = \int_V B_\phi^{\mathrm{T}} d N_\theta \,\mathrm{d}V, \quad K_{\theta\theta} = \int_V B_\theta^{\mathrm{T}} e^{\mathrm{T}} B_\theta \,\mathrm{d}V \\
&P_u = N_u^{\mathrm{T}} p, \quad P_\phi = N_\phi^{\mathrm{T}} q_e, \quad P_\theta = N_\theta^{\mathrm{T}} q_{\mathrm{t}}
\end{aligned} \tag{31}$$

Globally assembling the Eq. (30) and imposing geometric (essential) boundary conditions, the coupled linear equations can be solved. Nodal unknowns of displacement, electric potential, and temperature are determined. Through the constitutive relations, stresses, electric displacement, and heat flux are computed. Although the in-plane stresses can be predicted accurately within the capability of the present finite element, the accurate and reliable prediction of transverse stresses requires a post-process routine.

In the post-processing, transverse shear and normal stresses are obtained by integrating 3-D local stress equilibrium equations through the thickness of laminates. 3-D local stress is shown from Eq. (32).

$$\sigma_{xz} = -\int \sigma_{xx,x} + \sigma_{xy,y}\,\mathrm{d}z \tag{32a}$$

$$\sigma_{yz} = -\int \sigma_{yx,x} + \sigma_{yy,y}\,\mathrm{d}z \tag{32b}$$

$$\sigma_{zz} = -\int \sigma_{zx,x} + \sigma_{zy,y}\,\mathrm{d}z \tag{32c}$$

In Eq. (32), derivatives of strain and curvature are obtained by the idea of differential quadrature method (Zhong, 2001).

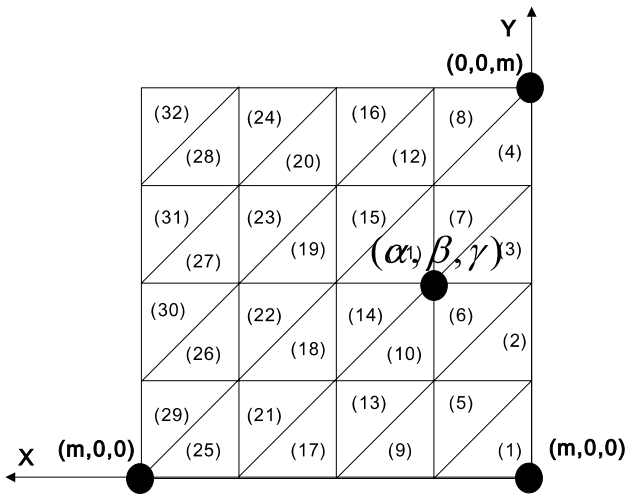


Fig. 4. Mesh configuration of differential quadrature for the computation of interlaminar stresses.

Partial derivative of a function with respect to a space variable at a grid point is approximated by the weighted linear summation of function values at all grid points within the local region. The domain is shown in Fig. 4. Thus,

$$D_n\{f(x,y)\}_{\alpha\beta\gamma} = \sum_{j=0}^{m}\sum_{i=0}^{m-j} C^{(n)}_{\alpha\beta\gamma,pqr} f_{pqr} \quad (p,q,r) = (m-i-j,i,j) \tag{33}$$

where $C^{(n)}_{\alpha\beta\gamma,pqr}$ are the weighting coefficients related to the function values $f_{pqr}$ and they are given as

$$C^{(x)}_{\alpha\beta\gamma,pqr} = \left[\frac{\partial L_1}{\partial x} \quad \frac{\partial L_2}{\partial x} \quad \frac{\partial L_3}{\partial x}\right] \begin{Bmatrix} \frac{\partial f_{pqr}}{\partial L_1} \\ \frac{\partial f_{pqr}}{\partial L_2} \\ \frac{\partial f_{pqr}}{\partial L_3} \end{Bmatrix}_{\alpha\beta\gamma} = \left[\frac{b_1}{2\Delta} \quad \frac{b_2}{2\Delta} \quad \frac{b_3}{2\Delta}\right] \begin{Bmatrix} \frac{\partial \bar{f}_p}{\partial L_1}\bar{f}_q\bar{f}_r \\ \bar{f}_p\frac{\partial \bar{f}_q}{\partial L_1}\bar{f}_r \\ \bar{f}_p\bar{f}_q\frac{\partial \bar{f}_r}{\partial L_1} \end{Bmatrix}_{\alpha\beta\gamma} \tag{34}$$

where $f_{pqr}|_{\alpha\beta\gamma} = \bar{f}_p(L_1)|_{L_1=\alpha/m}\bar{f}_q(L_2)|_{L_2=\beta/m}\bar{f}_r(L_3)|_{L_3=\gamma/m} = \delta_{\alpha p}\delta_{\beta q}\delta_{\gamma r}$ $(0 \leqslant p,q,r \leqslant m)$.

The auxiliary function is given as,

$$\bar{f}_p(L_1) = \begin{cases} \prod_{k=1}^{p} \frac{mL_1-k+1}{k}, & 1 \leqslant p \leqslant m \\ 1, & p = 0 \end{cases} \tag{35}$$

From Eq. (33), the derivatives of function $f(x,y)$ at the point $(x,y)$ can be easily computed from the information of nodal values within local region near the point $(x,y)$.

## 4. Numerical examples

To assess the performance and the validity of the developed finite element of the present study, the deformation and stresses are obtained in the smart composite plate under doubly sinusoidally varying mechanical, thermal, and electric inputs. The results of the present finite element are compared with the analytical solutions (Cho and Oh, submitted for publication) based on the same model and the ANSYS solutions based on the 8-node brick element.

Constitutive relations are given in Eqs. (2)–(4) account for full coupling between mechanical, thermal and electric fields. Eqs. (5) and (6) are used to replace the strains and the electric fields in Eqs. (2) and (3) by their expressions in terms of the displacements and electric potentials. Eq. (4) may not be used for steady-state problems.

The response of the decoupled theory has been studied in the previous paper (Cho and Oh, 2002). The previous study (Cho and Oh, 2002) demonstrated that the transverse normal deformation effect cannot be neglected under thermal and electric loads. In the present numerical study, three types of decoupled/coupled problems are considered. They are decoupled mechanical-electric-thermal problem, and coupled mechanical-electric problem, and fully coupled thermo-electric-mechanical problem. In the present numerical examples, 1/4 domain and $16\times16$ mesh configuration is used for the whole computations.

### 4.1. Decoupled mechanical-electric1-thermo problems

Mechanical, thermal, and electric loads are considered respectively. For the numerical evaluation of the performance of the proposed model, rectangular plates under simply supported boundary conditions are considered. In the mechanical loading case, transverse loading is assumed as doubly sinusoidal. In the thermal loading case, temperature is assumed sinusoidal in the reference plane and assumed linear through the thickness. In the electric loading case, electric field is also assumed as doubly sinusoidal in the piezoelectric layer. The material properties of the numerical examples are given in Table 1. In the mechanical loading case, five-layered cross-ply laminates are considered. As shown in the Fig. 5, in the thick laminate configurations ($a/h = 4$), the deformations and stresses including transverse shear and normal stresses are predicted very accurately in the present finite element analysis compared to the analytical solutions of the present theory (Cho and Oh, 2002). The present finite element result is correlated well with that of analytical solution. Same order of accuracy of the present theory can also be obtained by the EHOPT (efficient higher order plate theory) with cubic zig-zag in-plane displacement field (Cho and Parmerter, 1992, 1993) under the plane stress assumption. Transverse shear and normal stresses are obtained by integrating 3-D local stress equilibrium equations through the thickness of laminates.

The thermal loading cases are given in Fig. 6. The finite element result of thick case ($L/h = 4$) with material properties given in Table 1 is compared to the analytical solutions of present theory (Cho and Oh, 2002). The transverse shear stresses vary in the complicated zig-zag pattern through the thickness. The present theory provides very accurate solutions for deformations and transverse stresses as well as the in-plane stresses. The inclusion of transverse normal stress and strain effects makes the prediction of laminates under thermal loading accurate in the present model.

In the thermo-mechanical examples, the accuracy and efficiency of the present finite element have been demonstrated. The number of primary variables of the present model does not depend upon the number of layers. It has only two more primary variables compared to those of the previous EHOPT because it

Table 1
Material properties used in numerical examples

| Material property [0/90/0/90/0] |
|---|
| $E_L = 172.37 \times 10^9$ Pa |
| $E_T = 6.895 \times 10^9$ Pa |
| $G_{LT} = 3.4475 \times 10^9$ Pa |
| $G_{TT} = 1.379 \times 10^9$ Pa |
| $\nu_{LT} = 0.25$ |
| $\nu_{TT} = 0.25$ |
| $\alpha_{LL} = 1 \times 10^{-8}$ /°C |
| $\alpha_{TT} = 1123 \times 10^{-6}$ |

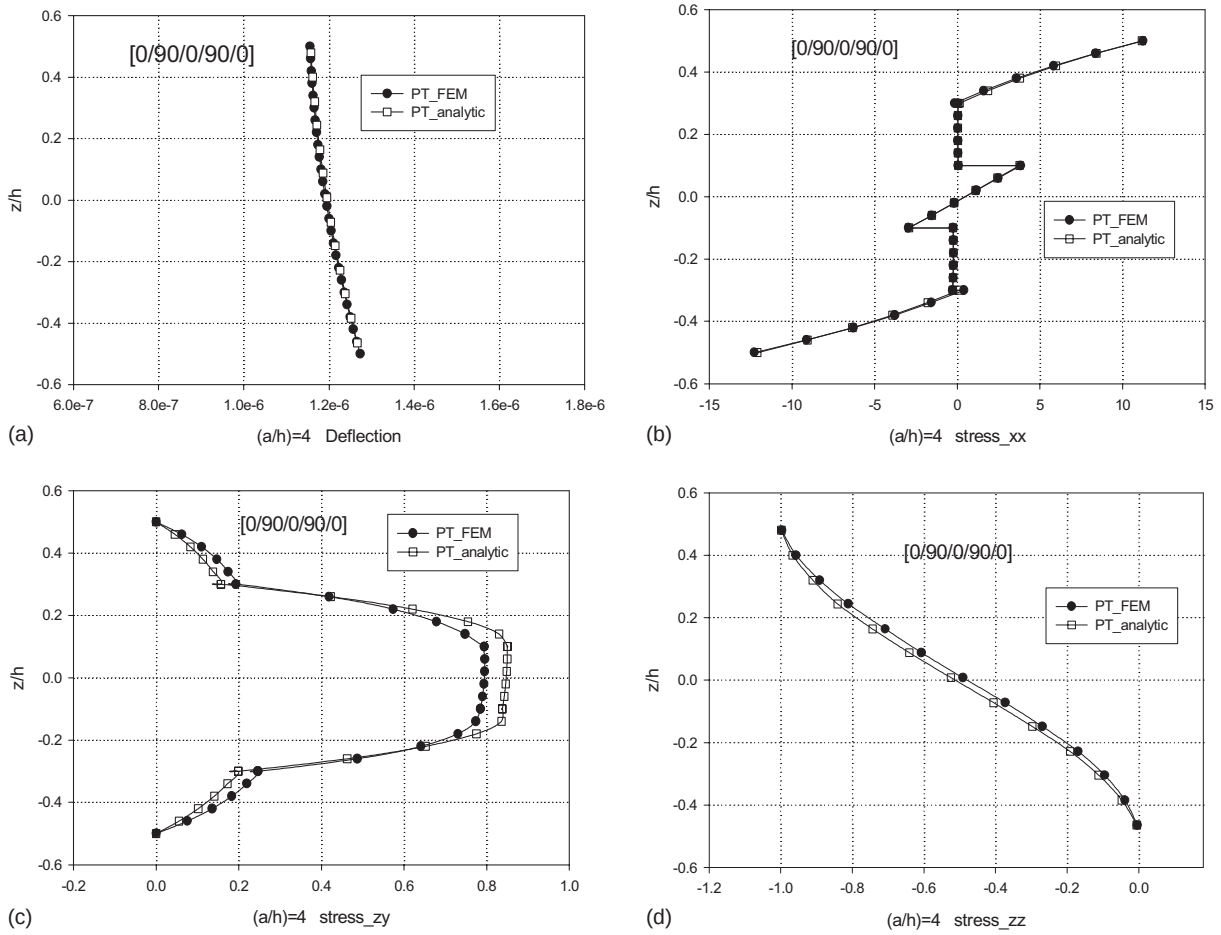


Fig. 5. (a) Deflection for mechanical loading, (b) in-plane stress for mechanical loading, (c) transverse shear stress for mechanical loading, (d) transverse normal stress.

includes transverse normal deformation effect through the thickness of laminates. To avoid more complexity of the displacement field, the transverse normal stress continuity conditions through the thickness are not imposed in the present modeling.

The electric loading cases are given in Fig. 7. Model of composite laminates with surface bonded piezoelectric actuators, subjected to externally applied electric field loads, is considered.

Figs. 5(a), 6(a), 7(a) depicts deflection for mechanical-thermo-electric loading case. In the mechanical loading case, deflection through the thickness is almost constant. In the thermal loading case and the electric loading case, the deflections change considerably through the thickness of plates. It is observed that transverse normal effect is significant in the thermal and electric loading cases.

### *4.2. Coupled mechanical-electric problems*

Simply supported square plate with [piezo(sensor)/0/90/0/piezo(actuator)] layup is considered. The mechanical loading is doubly sinusoidal and it is applied at the top bounding surface. The material

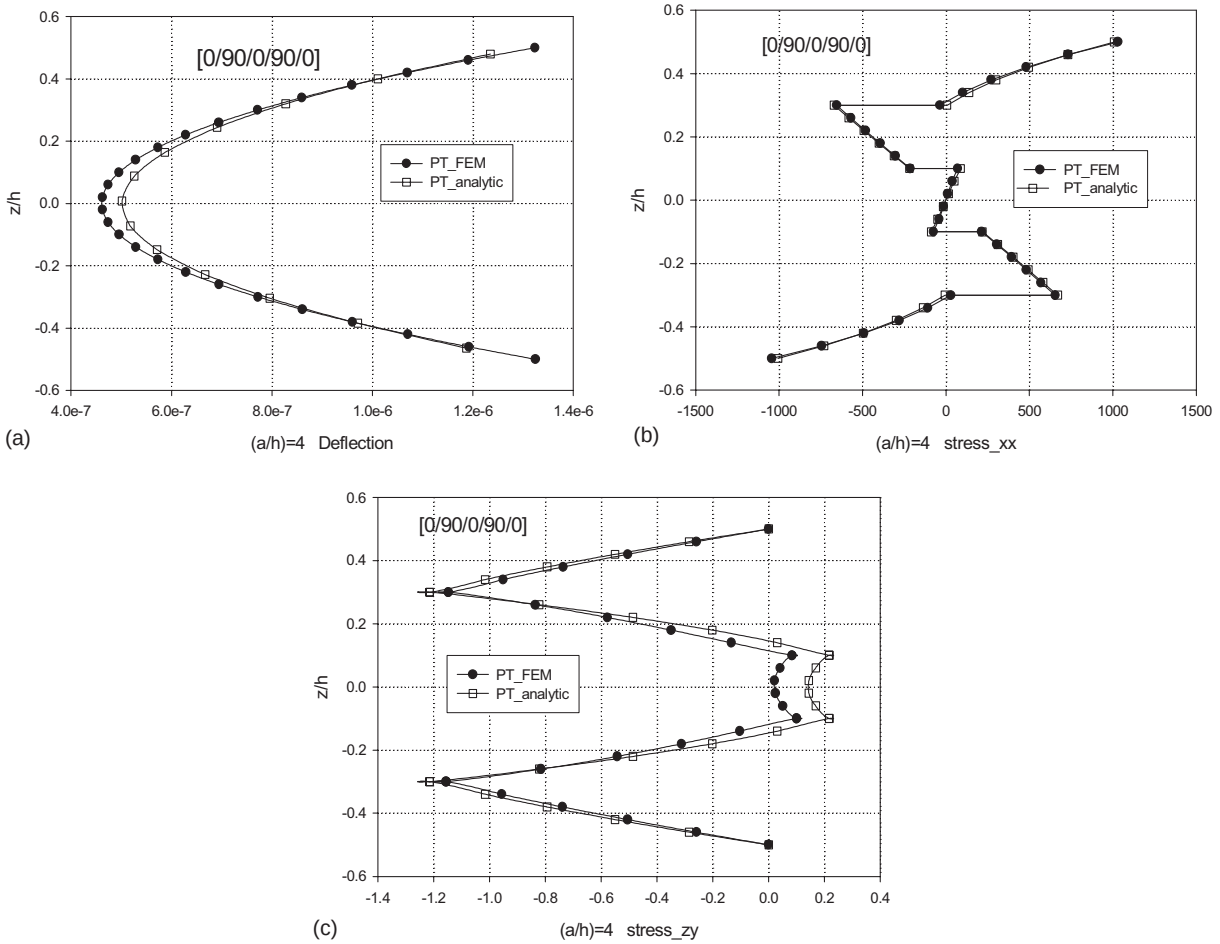


Fig. 6. (a) Deflection for thermal loading, (b) in-plane stress for thermal loading, (c) transverse shear stress for thermal loading.

properties for this case are given in Table 2. Applied mechanical load is 6894.7 Pa and the voltage 100 V is applied at the piezo-actuator located at the bottom of the laminate. The 3-D elasticity solutions for mechanical-electric coupled problems can be found in Ray et al. (1993) and Sheikh et al. (2001).

As shown in Fig. 8(a), in the thick plate ($S = 4$), the out-of-plane displacement has parabolic pattern through the thickness and the prediction of the present finite element based on higher order zig-zag model correlates very well with that of the analytical solutions. As shown in Fig. 8(b), in the moderate thick case ($S = 10$), the deflection is almost uniform through the thickness. Once more, the results of finite element are correlated very well with those of analytical solutions. Fig. 8(c) illustrates that the deflection of closed circuit has larger value than that of open circuit. In other words, closed circuit deflection is larger because mechanical energy in the coupled theory (open circuit) is divided into thermal energy and electrical energy. The deflection of the coupled one is smaller than that of closed circuit. Open-circuit condition gives the applied charge density on the surface to zero. Closed-circuit condition make an imposed potential equal to zero. Fig. 8(d) indicates that in-plane stress of closed circuit compared with those by the open circuit. There is no significant difference of stress distribution through the thickness. It is observed from Fig. 8(e) that transverse shear stress using FEM analysis is agree well with analytic one of present theory.

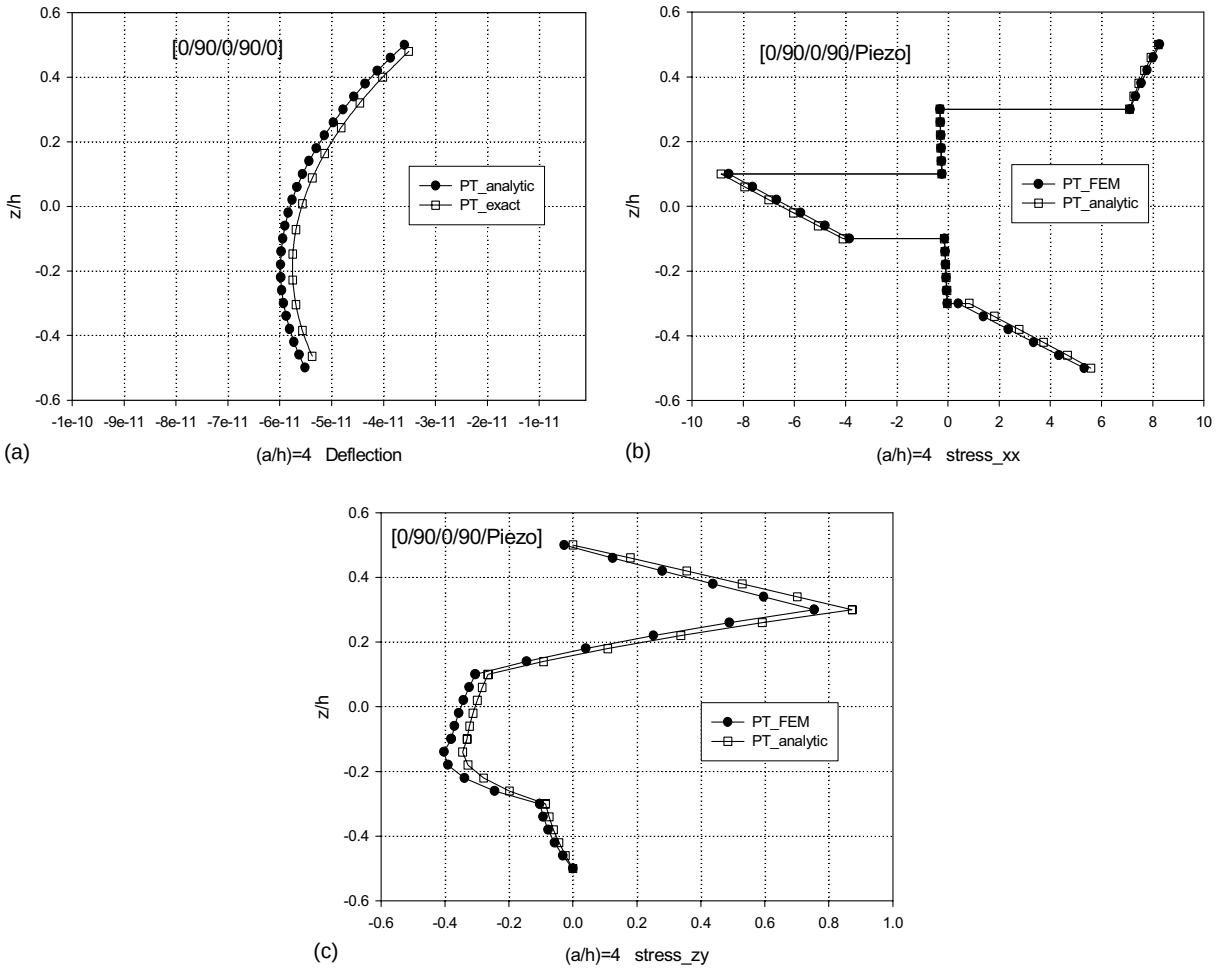


Fig. 7. (a) Deflection for electric loading, (b) in-plane stress for electric loading, (c) transverse shear stress for electric loading.

Table 2
Material properties of the graphite–epoxy and PZT layers

| PVDF layer | Graphite–epoxy layer |
|---|---|
| $E_1 = E_2 = E_3 = 2 \times 10^9$ Pa | $E_1 = 172.37 \times 10^9$ Pa |
| $v = 0.29$ | $E_2 = E_3 = 6.895 \times 10^9$ Pa |
| $e_{31} = e_{32} = 0.0046$ C/m$^2$ | $G_{12} = G_{13} = 3.4475 \times 10^9$ Pa |
| $e_{33} = e_{24} = e_{15} = 0$ | $G_{23} = 1.379 \times 10^9$ Pa |
| $b_{11} = b_{22} = b_{33} = 0.1062 \times 10^{-9}$ f/m | $v = 0.25$ |
| | $b_{11} = b_{22} = b_{33} = 8.85 \times 10^{-3}$ f/m |

### 4.3. Coupled thermo-electric-mechanical problem

For the analysis of fully coupled case, a problem with the prescribed bounding surface heat flux is considered. Heat flux $q_t = 1000$ W/m$^2$ is applied on the top surface of the plate. The bottom surface is

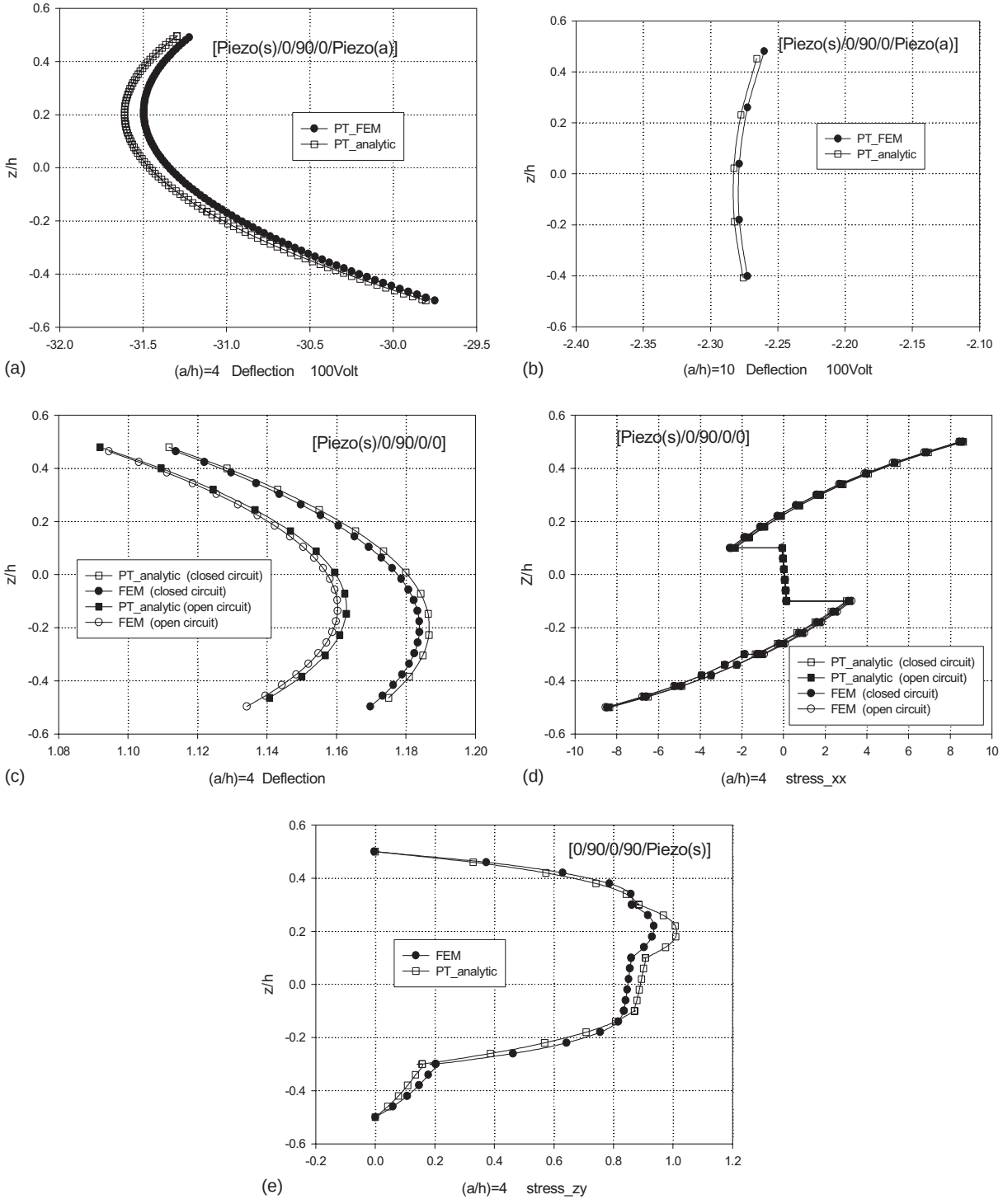


Fig. 8. (a) M–E deflection for electric loading, (b) M–E deflection for electric loading, (c) M–E coupled deflection for mechanical loading, (d) M–E coupled in-plane stress for mechanical loading, (e) M–E coupled transverse shear stress for mechanical loading.

Table 3
Material properties of the graphite-epoxy and PZT layers

| PZT layer | Graphite–epoxy layer |
|---|---|
| $E_1 = E_2 = E_3 = 63 \times 10^9$ Pa | $E_1 = 144.23 \times 10^9$ Pa |
| $G_{12} = G_{13} = G_{23} = 24.6 \times 10^9$ Pa | $E_2 = E_3 = 9.65 \times 10^9$ Pa |
| $v = 0.28$ | $G_{12} = G_{13} = 4.14 \times 10^9$ Pa |
| $\alpha_{11} = \alpha_{22} = \alpha_{33} = 0.9 \times 10^{-6}$ /°C | $G_{23} = 3.45 \times 10^9$ Pa |
| $d_{31} = d_{32} = 150 \times 10^{-12}$ m/V | $v = 0.3$ |
| $d_{33} = -336.8 \times 10^{-12}$ m/V | $\alpha_{11} = 1.1 \times 10^{-6}$ /°C |
| $d_{24} = 0$ | $\alpha_{22} = \alpha_{33} = 25.2 \times 10^{-6}$ /°C |
| $d_{15} = 0$ | $\kappa_{11} = 4.48$ W/m °C |
| $b_{11} = b_{22} = 15.3 \times 10^{-9}$ f/m | $\kappa_{22} = \kappa_{33} = 3.21$ W/m °C |
| $b_{33} = 15.0 \times 10^{-9}$ f/m | |
| $d_3 = 20 \times 10^{-6}$ C/m$^2$ °C | |
| $\kappa_{11} = \kappa_{22} = \kappa_{33} = 2.1$ W/m °C | |

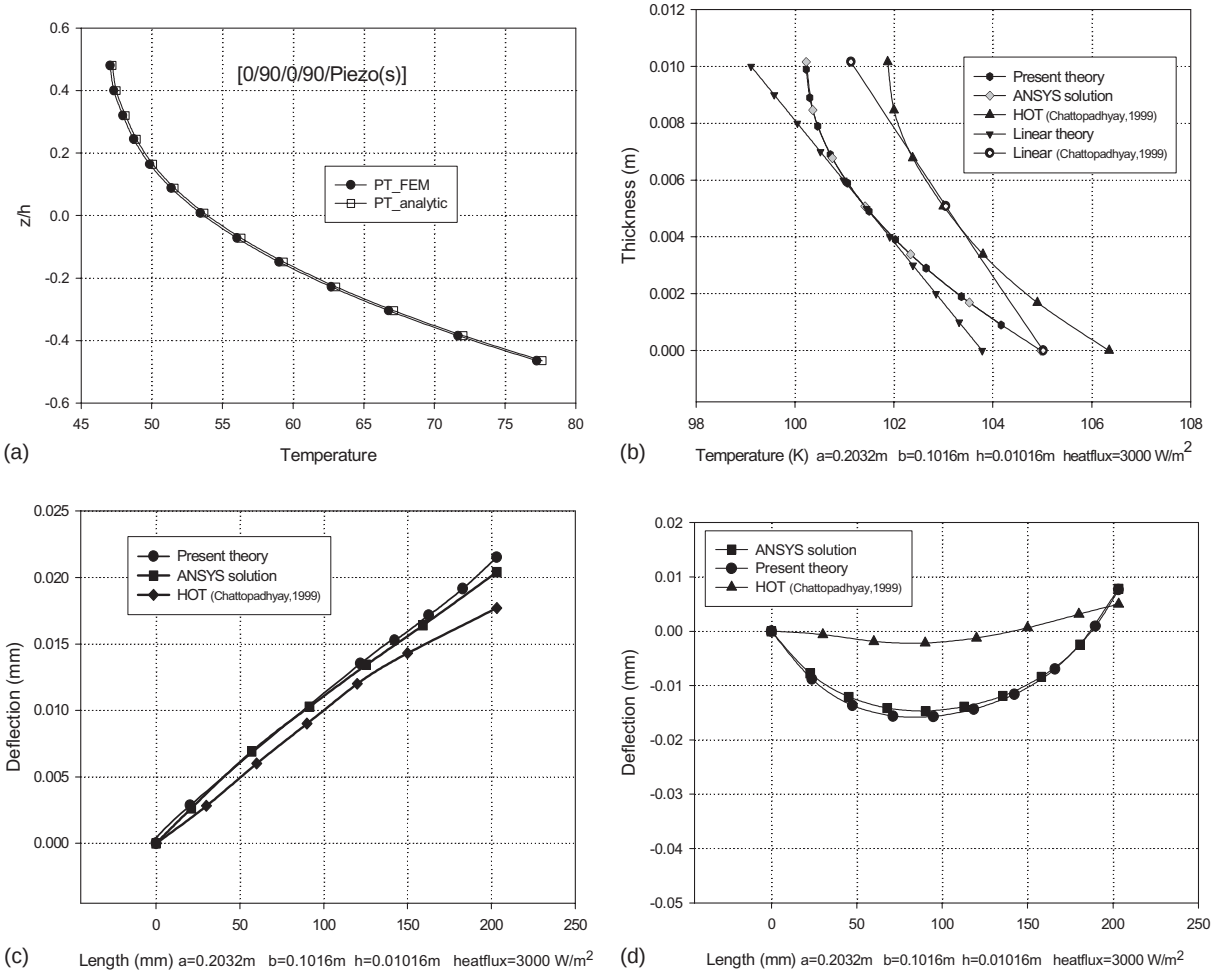


Fig. 9. (a) Temperature field from the heat equation, (b) temperature field through the thickness, (c) deflection according to the length under heat flux loading, (d) deflection according to the center length under heat flux loading.

adiabatic, i.e. $q_b = 0$ W/m$^2$. The layup configuration is given as [0/90/0/90/piezo(sensor)]. The material properties for this case are given in Table 3.

The temperature profile is shown in Fig. 9(a). Through-the-thickness temperature distribution is obtained by solving simultaneously coupled heat equation, mechanical equilibrium equation and electro-static equation. It shows a smooth distribution through the thickness except the piezo-actuator layer, where the high temperature gradient is observed. If we consider the case with severe changes of thermal property through the thickness such as the sandwich or hybrid composite plate, the zig-zag assumed temperature field in the present theory may strongly demonstrate its efficiency and accuracy.

To assess the validity of temperature field, the present finite element results are compare to those of the previously reported work (Chattopadhyay et al., 1999). The example given in Chattopadhyay et al. (1999) was adopted for the comparison purpose. The numerical model is a clamped square plate with unidirectional [0] layup. Heat flux $q_t = 3000$ W/m$^2$ is applied on the top surface. Geometric data of the example is given as length $a = 0.2032$ m, width $b = 0.1016$ m and thickness $h = 0.01016$ m.

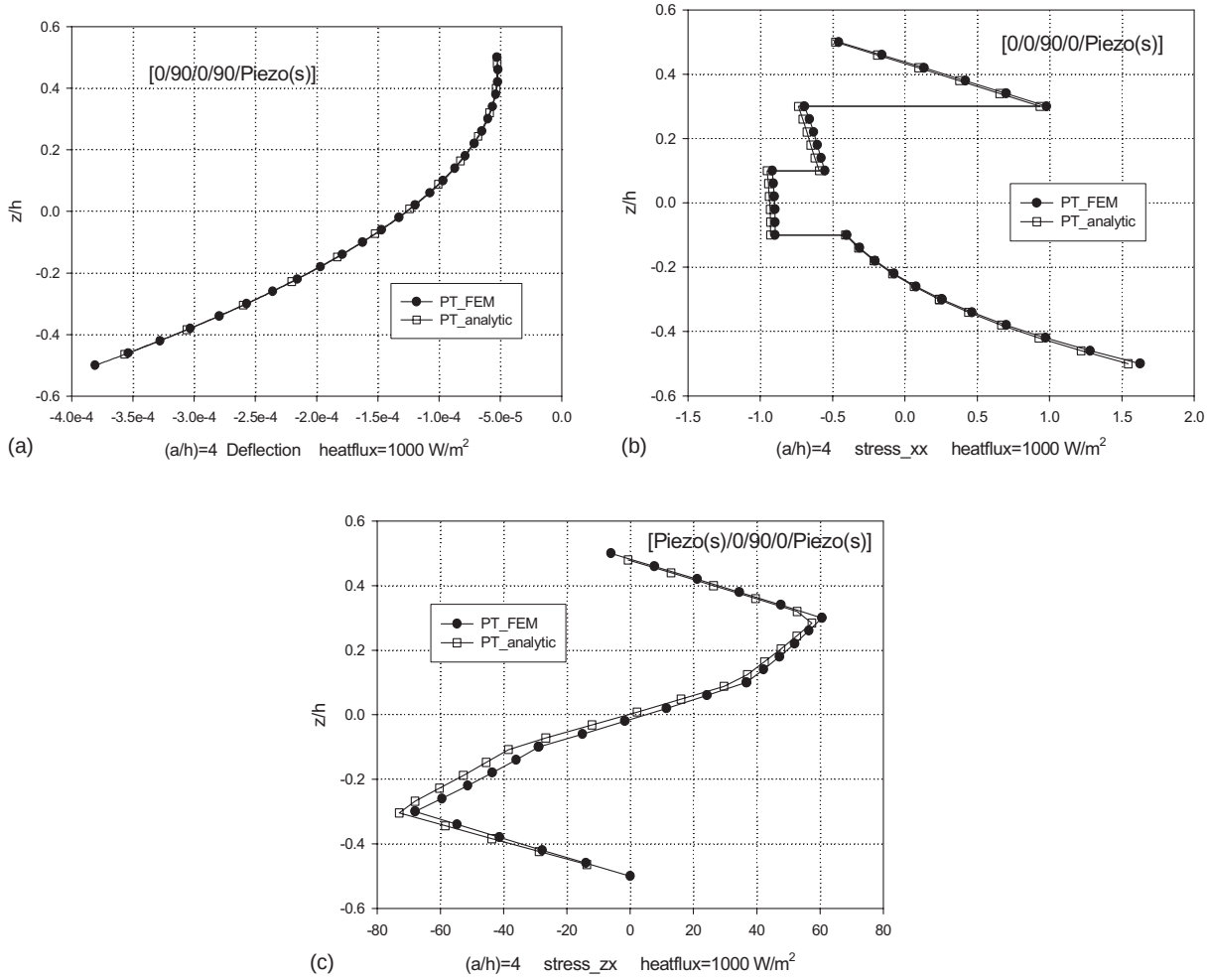


Fig. 10. (a) Fully coupled deflection for heat flux loading, (b) fully coupled in-plane stress for heat flux loading, (c) fully coupled transverse shear stress for heat flux loading.

The finite element solutions of the present theory agree very well with 3-D ANSYS solutions. However, the temperature field of HOT proposed by Chattopadhyay et al. (1999) deviated erroneously from the ANSYS results performed by us as shown in Fig. 9(b)–(d). Neither the results of HOT proposed by Chattopadhyay et al. (1999) nor ANSYS results performed by Chattopadhyay et al. (1999) are based on the fully refined meshes. They used two coarse meshes to compare the results of their model with those of ANSYS. Both of them deviate significantly from the converged ANSYS results and also from the present finite element solutions of zig-zag cubic model. More refined meshes are required to obtain the converged solutions of both their model and their ANSYS results. In our simulations, to obtain converged solution, $60\times20\times6$ mesh configuration is used for 8-node brick element of ANSYS software. The $16\times16$ mesh configurations are used for the converged solution of the present finite element analysis. The temperature distribution by the linear profile assumption through the thickness of the plates is shown in Fig. 9(b). The result of fully refined mesh is marked as ''Linear theory'' and the result reported by Chattopadhyay et al. (1999) is marked as ''Linear (Chattopadhyay et al., 1999)''.

Fig. 9(c) depicts the transverse deflection along the $y$-axis. The prediction of the deflection by the present finite element agrees well with the results of ANSYS. It is observed that the maximum deflection occurs at the plate tip. Also, as shown in Fig. 9(d), deflection of midline along the $y$-axis is correlated very well with that of the ANSYS solutions. Thus the present results should serve as a reference data when the performances of prediction of thermo-electric-mechanical behaviors of newly developed models are required.

As shown in Fig. 10, in the case of thick plate ($S = 4$), the prediction of the out-of-plane displacement, in-plane stress and transverse shear stress through the thickness by the present higher order zig-zag element agrees very well to those of analytical solutions.

## 5. Conclusion

In the present study, a three-node triangular finite element based on cubic zig-zag plate theory has been developed in order to analyze the behavior of the smart structure with piezo-layers.

By imposing transverse shear stress free condition of top and bottom surfaces and interface continuity conditions between layers, layer-dependent displacement variables were eliminated. In the similar way, by imposing top and bottom surface heat flux boundary conditions and interface heat flux continuity conditions between layers, the temperature unknowns reduced to the temperature degrees of freedom of reference surface. Thus the final form of displacement and temperature fields has only reference primary variables. Thus only layer-dependent degrees of freedom come from the electric potential degrees of freedom. However, the formulation still keeps the efficiency since the number of the piezoelectric layers is not so large in the practical applications.

Through the numerical examples of decoupled/coupled responses, the transverse normal deformation effect is not negligible in the situations that electric and thermal loads are applied. The present finite element based on the zig-zag higher order theory demonstrated its performance in predicting deformations and interlaminar stresses because it includes the effect of transverse normal deformation. However, for the accurate prediction of interlaminar stresses, the integration of 3-D local stress equilibrium equations is required in the present theory as other higher order plate theories do. The idea of differential quadrature method is utilized to calculate the higher order derivatives of primary variables in the 3-D stress equilibrium equations. The differential quadrature works well in the triangular mesh configurations to evaluate interlaminar stresses. The present finite element can serve as a powerful tool to predict fully-coupled thermo-electric-mechanical behavior of smart composite plates with embedded or attached piezo-electric sensor and/or actuator.

## Acknowledgement

This work was supported by Micro Thermal System Research Center of Seoul National University.

## References

Ali, J.S.M., Bhaskar, K., Varadan, T.K., 1999. A new theory for accurate thermal/mechanical flexural analysis of symmetric laminated plates. Composite Structures 45, 227–232.

Chattopadhyay, A., Li, J., Gu, H., 1999. Coupled thermo-piezoelectric-mechanical model for smart composite laminates. AIAA Journal 37 (12), 1633–1638.

Cho, M., Oh, J., 2001. Higher order zig-zag theory for fully coupled thermo-electric-mechanical smart composite plates. AIAA/ASME/ASCE/AHS/ASC, 42nd SDM Conference, Seattle, WA, 2001, AIAA Paper no. 2001–1403, pp. 1–10.

Cho, M., Oh, J., 2002. Higher order zig-zag plate theory under thermo-electric-mechanical loads combined. Composites B 34 (1), 67–82.

Cho, M., Oh, J., submitted for publication. Higher order zig-zag theory for fully coupled thermo-electric-mechanical smart composite plates. International Journal of Solids and Structures.

Cho, M., Parmerter, R.R., 1992. An efficient higher-order plate theory for laminated composites. Composite Structures 20, 113–123.

Cho, M., Parmerter, R.R., 1993. Efficient higher-order composite plate theory for general lamination configurations. AIAA Journal 31, 1299–1306.

Cho, M., Parmerter, R.R., 1994. Finite element for composite plate bending based on efficient higher order theory. AIAA Journal 32 (11), 2241–2248.

Crawley, E.F., 1987. Use of piezoelectric actuators as elements of intelligent structures. AIAA Journal 25 (10), 1373–1385.

Franco Correia, V.M., Aguiar Gomes, M.A., Suleman, A., Mota Soares, C.M., Mota Soares, C.A., 2000. Modeling and design of adaptive composite structures. Computer Methods in Applied Mechanics and Engineering 185, 325–346.

Ha, S.K., Keilers, C., Chang, F., 1992. Finite element analysis of composite structures containing distributed piezoceramic sensors and actuators. AIAA Journal 30 (3), 772–780.

Lee, C.K., 1990. Theory of laminated piezoelectric plates for the design of distributed sensors/actuators. Part I: governing equations and reciprocal relationships. Journal of the Acoustical Society of America 87 (3), 1144–1158.

Mitchell, J.A., Reddy, J.N., 1995. A refined hybrid plate theory for composite laminates with piezoelectric laminate. International Journal of Solids Structure 32 (16), 2345–2367.

Ray, M.C., Bhattacharya, R., Samanta, B., 1993. Exact solution for static analysis of intelligent structures. AIAA Journal 31 (9), 1684–1691.

Reddy, J.N., Robbins Jr., D.H., 1994. Theories and computational models for composite laminates. Applied Mechanics Reviews 47 (6), 147–169.

Saravanos, D.A., Heyliger, P.R., Hopkins, D.A., 1997. Layerwise mechanics and finite element for the dynamic analysis of piezoelectric composite plates. International Journal of Solids Structure 34 (3), 359–378.

Sheikh, A.H., Topdar, P., Halder, S., 2001. An appropriate FE model for through-thickness variation of displacement and potential in thin/moderately thick smart laminates. Composite Structures 51, 401–409.

Specht, B., 1988. Modified shape functions for the three-node plate bending element passing the patch test. International Journal for Numerical Methods in Engineering 26, 705–715.

Zhong, H., 2001. Triangular differential quadrature and its application to elastostatic analysis of Reissner plates. International Journal of Solids Structure 38, 2821–2832.